



Alexandria University  
**Alexandria Engineering Journal**

[www.elsevier.com/locate/aej](http://www.elsevier.com/locate/aej)  
[www.sciencedirect.com](http://www.sciencedirect.com)



# Effect of non-conjugate and conjugate condition on heat transfer from battery pack

Imran Mokashi <sup>a,b</sup>, Asif Afzal <sup>c,\*</sup>, Qasem Al-Mdallal <sup>c,\*</sup>, L. Syam Sundar <sup>d</sup>,  
 Sher Afghan Khan <sup>a</sup>, Nur Azam Abdullah <sup>a</sup>, Muhammad Hanafi Azami <sup>a</sup>,  
 C Ahamed Saleel <sup>e</sup>

<sup>a</sup> Department of Mechanical Engineering, International Islamic University Malaysia, Kuala Lumpur, Malaysia

<sup>b</sup> Department of Mechanical Engineering, Bearys Institute of Technology, (Affiliated to Visvesvaraya Technological University), Mangaluru, Karnataka, India

<sup>c</sup> Department of Mathematical Sciences, United Arab Emirates University, P. O. Box 15551, Al Ain, United Arab Emirates

<sup>d</sup> Department of Mechanical Engineering, University of Aveiro, 3810-193 Aveiro, Portugal

<sup>e</sup> Department of Mechanical Engineering, College of Engineering, King Khalid University, PO Box 394, Abha 61421, Saudi Arabia

Received 22 May 2021; revised 9 August 2021; accepted 14 August 2021

## KEYWORD

Battery;  
 Li-ion;  
 Temperature;  
 Conjugate;  
 Heat transfer;  
 Conductivity ratio

**Abstract** Li-ion battery packs provide high energy density but with a concern of thermal management. Hence cooling mechanism is necessary to have a good life and reliability on the battery system. The main objective of this article is to investigate the effect of conjugate and non-conjugate boundary conditions on battery pack heat transfer characteristics. In conjugate conditions, coolant flow is considered with heat flux continuity at the battery and fluid interface. In non-conjugate condition, just convection condition is adopted. The finite volume method is adopted for the numerical analysis, and a code is written for computations of the governing equations. Effects of different parameters like heat generation, conductivity ratio, coolants, and Biot number on temperature distribution in the battery pack are analyzed. The maximum temperature contours are located near the top end of the battery, whereas at the bottom end, the battery's temperature is low. Such high and low-temperature regions in the battery pack create uneven thermal stresses, resulting in battery failure. To have better performance results for the battery system, one should maintain the proper balance of thermal conductivity between the solid and fluid domains. From comparative analysis it is found that the non-conjugate condition gives the temperature distribution in battery to be of symmetrical nature and more uniform. Practically, this is not true which is confirmed by the realistic conjugate condition where the high temperature zones are closer to the trailing edge of the battery pack. Liquid metals and nanofluids provide a much safer operating temperature of the pack where the maximum temperature is well below the critical temperature. The application of conjugate

\* Corresponding authors.

E-mail addresses: [asif.afzal86@gmail.com](mailto:asif.afzal86@gmail.com) (A. Afzal), [q.almdallal@uaeu.ac.ae](mailto:q.almdallal@uaeu.ac.ae) (Q. Al-Mdallal), [sakhan06@gmail.com](mailto:sakhan06@gmail.com) (S.A. Khan).

Peer review under responsibility of Faculty of Engineering, Alexandria University.

<https://doi.org/10.1016/j.aej.2021.08.042>

1110-0168 © 2021 THE AUTHORS. Published by Elsevier BV on behalf of Faculty of Engineering, Alexandria University.

This is an open access article under the CC BY-NC-ND license (<http://creativecommons.org/licenses/by-nc-nd/4.0/>).

Please cite this article in press as: I. Mokashi et al., Effect of non-conjugate and conjugate condition on heat transfer from battery pack, Alexandria Eng. J. (2021), <https://doi.org/10.1016/j.aej.2021.08.042>

condition for battery thermal analysis leads to be have an insight of the hotspot zones accurately which are operated using conventional fluids mentioned in this work.

© 2021 THE AUTHORS. Published by Elsevier BV on behalf of Faculty of Engineering, Alexandria University. This is an open access article under the CC BY-NC-ND license (<http://creativecommons.org/licenses/by-nc-nd/4.0/>).

## 1. Introduction

Electric and Hybrid vehicles depend on Li-ion batteries (LIB) as a reliable energy source needed for automotive applications. The high energy to volume ratio and charging/discharging stability rate associated with LIB make them distinguished in electric vehicles. During adverse energy demands, the amount of heat produced within the battery pack can considerably affect the battery performance. Thus a proper thermal management system is needed to enhance the operational quality and safety of these batteries. The paper presents a complete guide in selecting coolant for an exhaustive set of criteria involving heat generation, Biot number, Prandtl number, Reynolds number, and conductivity ratio.

Extensive research has been done in the battery thermal management system (BTMS). The susceptibility of a battery pack to thermal runaway during peak energy demands, charging/discharging and accidents, causes degradation of the electrochemical battery components. The solutions proposed for different aspects affecting the battery performance have been compiled for an elaborated review.

Maleki et al. [1] conducted an experimental investigation to understand the thermal performance of Sony US-18650 LIB with and without the use of electrolytes. The use of electrolytes reduced the resistance to thermal contact. That enhanced the thermal conductivity. Hatchard et al. [2] developed a one-dimensional numerical model to predict the response of cells with different shapes and electrolytes. The model predictions are confirmed with the results obtained from the conventional exposure to oven testing employed to test new cells for their response to high temperatures. That dramatically saves time and money by accurately predicting thermal responses for different cell shapes, materials, and electrolytes without physically making the cell. An extended study of the same was conducted by Kim et al. [3] using a 3-dimensional cylindrical model to study the hot spot propagation through the cell when exposed to high temperatures in an oven test. The heat dissipation was found to take place effectively in small-sized cells than in large cells. Guo et al. [4] researched the effects of  $Q_{gen}$ , internal conduction, convection, and heat dissipation externally to understand the temperature distribution in a 3-dimensional LIB. The geometrical aspect, which is significant in large LIB used in electric vehicles, was analyzed.

Mahmud et al. [5] used a 3-dimensional CFD model to predict the thermal behavior of LIB. The heat dissipation was enhanced by employing reciprocating airflow over cylindrical cells. The reduction in battery temperature was increased by 4 °C, and for a reciprocating flow period of 2 min, the maximum temperature was reduced by 1.5 °C in comparison to unidirectional flow. Karimi et al. [6] organized their research in battery thermal management systems to study the issues related to thermal abuse in LIB available commercially. A lumped capacitance numerical model arranged in U and Z patterns were analyzed for effective heat dispersion. The use of

coolant was found to be effective in heat transfer from the battery cell. Karimi and Li [7] studied the various possibilities to maintain battery temperatures within a safe range. Cooling techniques aided with different battery configurations were researched. It was commented that forced convection could expedite the cooling of LIB and cost-effectively maintain a uniform temperature.

Samba et al. [8] studied heat generation parameters obtained experimentally and a transient 2-D thermal model. The comparison was made for different current charging/discharging rates. The experimental and numerical simulation results are in close agreement. Burheim et al. [9] presented an extensive study on heat generation during charging/discharging. The experimental evaluation of commercial and non-commercial LIB electrode material was done with and without considering electrolytes. A Fourier thermal model was used to interpret this data to conclude charging/discharging temperature profiles. H. Park [10] attempted to provide an optimum solution for effectively cooling the battery pack by utilizing air in forced convection. He has commented that the uniform coolant distribution through the passages in the battery pack is pivotal in heat dissipation. He concluded that using a tapered manifold with pressure relief ventilation can provide the desired thermal management without any layout design change. Chiu et al. [11] experimentally investigated a thermal abuse condition of the battery pack when a nail is penetrated, causing a short circuit. The effect of mass and charge transfer was studied, and an electrochemical numerical model could accurately predict the thermal runaway. The temperature profiles obtained numerically and experimentally were well fitted. Choi et al. [12] have tried to present a simplistic battery cooling system by proposing a suitable design air-cooled. The convective transfer of heat gave considerable results in reducing the battery temperature during operation. Drake et al. [13] proposed a novel technique to measure the temperature of cylindrical cells in axial and radial directions. Anisotropy in temperature dissipation is developed in cylindrical Li-ion cells when arranged in a spiral configuration to give effective results. The radial heat transfer is found to be two orders less than axial direction heat dissipation. Huo et al. [14] analyzed the effects of coolant mass flow rate, the direction of flow, ambient temperature, and quantity of channels used to investigate the temperature dispersion in a 3-D thermal battery model. It was found that the increase in the number of mini channels and flow rate decreased the maximum temperature in the battery. They also remarked that an optimum flow rate of  $5 \times 10^{-4} \text{ kg s}^{-1}$  provides effective results. Javani et al. [15] employed a passive BTMS using porous foam as a Phase Change Material (PCM). The effects of varied discharge rates with and without PCM were compared with the simulation results obtained for a 4 cell submodule finite volume-based thermal response. The use of wet foam was found to give better battery temperature reduction than dry foam.

Panchal et al. [16] intended to study heat generation rate in a prismatic LIB at different discharge rates and boundary conditions. The surface of the battery with cathode material  $\text{LiFePO}_4$  was coated with aluminum for this study. It was observed that an increase in the discharge current and hence the discharge rate increased the rate of heat generation. Chalise et al. [17] considered a conjugate model of heat transfer to study the thermal management of LIB cells. An iterative analytical technique was used to solve the governing equations to determine the final temperature distribution. The cell geometry and material effect on the temperature distribution were examined. It was evaluated that the improvement in thermal conductivity of Li-ion cell, the coolant rate of flow can be reduced with effective cooling. Feng et al. [18] surveyed the thermal runaway condition caused by the Li-ion battery's mechanical, electrical, and thermal abuses during service. The chain reaction mechanism that causes the decomposition of battery parts was interpreted by developing a novel energy release chart. A 3-level concept for protection was proposed. Passive defense provision, runaway initiation alarm system, and thermal runaway propagation restriction methods were proposed. Li et al. [19] adopted experimental and numerical simulation techniques to study the voltage, current, and temperature distribution in a single battery and battery pack. Water cooling at low cycling rates was found to be an effective cooling system. Zhang et al. [20] conducted research on a computational 3-D model with a predetermined heat source and time period to study the thermal runaway caused by an internal short circuit. A safety regime diagram was configured to identify the zones of thermal runaway and safety zones. Similarly, much other Li-ion battery analyses using numerical approaches are reported in [21–30].

The computational flexibility of Spectral Element Method (SEM) in the analysis of electromagnetic radiation scenario as a comparative research study concerning the Finite Difference Method (FDM) and Finite Element Method (FEM) is reported by Mahariq [31–35] and his team. The SEM technique was observed to provide consistently accurate results for the unbounded 1-D and 2-D dielectric frequency domain, areas of application for similar error conditions [31–35].

The momentum, heat, and mass transfer in a Casson fluid impregnated with gyrotactic microorganisms under the influence of a magnetic field is explored in the work of Sohal and the team [36–41]. The temperature and concentration variations over linear and non-linear stretch were analyzed to develop an understanding for enhancing the system efficiency. Flow velocity was noted to retard with increased fluid and magnetic parameters and was found to increase with temperature and concentration improvement [36–41]. The convective heat transfer analysis through carbon nanotubes was conducted to study the thermal radiation incremental effect. The data perceived can be implemented in the devising of products [42–46].

The explorations endured in the study of battery thermal management has been concentrated on four aspects encompassing experimental or numerical simulation. The thermal limiting conditions were adopted for varying discharges in solid Li-ion battery. Simulation studies for variety of cell arrangements to optimize cooling in the battery modules are reported. It can be thereby clarified that conjugated heat transfer was incorporated by limited studies with constraints to types of fluid and their velocities, with the bounding conditions

of external flow, thermal conductivity, and rates of discharge solved analytically.

It is evident from the above literature survey that works carried out are experimental and numerical to study heat generation and dissipation. Various cell configurations, battery component materials, cooling systems, coolants, cooling directions, and flow rates have been investigated. The models are primarily analyzed with air or water as the coolants and either for conduction or convection heat transfer, natural or forced, except for a few. The present study is based on conjugate consideration of heat transfer at the cell-coolant interface, employing a wide range of coolants. Many coolants are considered for the temperature distribution analysis in thermal management of Li-ion cells. How the thermal performance is affected if non-conjugated condition is adopted is also explored in the beginning of the analysis. A comparison is made between these two important boundary conditions. A numerical model is developed and validated for this comparative study. This model is first validated and upon successful establishment it is used to get an insight in thermal nature of battery pack.

## 2. Mathematical formulation

A computation model is devised for the analysis of thermal performance of the Li-ion battery and at the battery-coolant common surface. Fig. 1a, resembles a battery module where it is cooled by flowing fluid. The conjugate thermal analysis model is represented by Fig. 1. The heat generation within these stacked batteries increases during charging/discharging. The convective heat extraction by coolant at the prismatic battery interface is portrayed in Fig. 1b. The symmetric heat transfer boundary condition is implemented, considering only half of the battery and coolant domains in the analysis, as depicted in Fig. 1c. This reduces the computation duration. The heat generation under constant charging and discharging for extended durations is reported to be uniform. The coolant flow velocity varies within 0.01 m/s to 12 m/s, thereby specifying the regime of fluid flow to be laminar. The circulation of coolant is maintained by the use of fan/air pump, which accounts for increased energy requirements.

A battery comprises of cathode, anode, electrolyte and partition materials which have micro thickness contrary to their height and width. The heat generation due to electrochemical reactions is complex to simulate a 3D realistic model. These attributes are dropped and a 2D model is incorporated for the thermal analysis of battery module to capitulate on the computational time. The generation of heat inside a battery is rigorous with enhanced energy demand and load. The heat dissipation occurs through the cell surface of the prismatic batteries. The energy demands specified in the US06 standards are  $6.8559 \times 10^3$  to  $29 \times 10^6$  W/m<sup>3</sup> for uphill conditions. The C-rate determines the heat generated per unit volume, ranging from  $67.8$  kW/m<sup>3</sup> to  $29 \times 10^6$  kW/m<sup>3</sup>. The dimensions of battery cell interpreted in the literature are length = 62 mm to 521 mm, width = 52 mm to 169 mm, and thickness = 0.185 mm to 27 mm. The cell thermal conductivity has been scribed as 0.02–30 W mK<sup>-1</sup>.

A 2-D computational model is developed to simulate the heat generation and transfer by conjugate mode of heat transfer at the interface. By symmetrical boundary condition along the y-axis, only one-half of the battery and fluid (coolant)

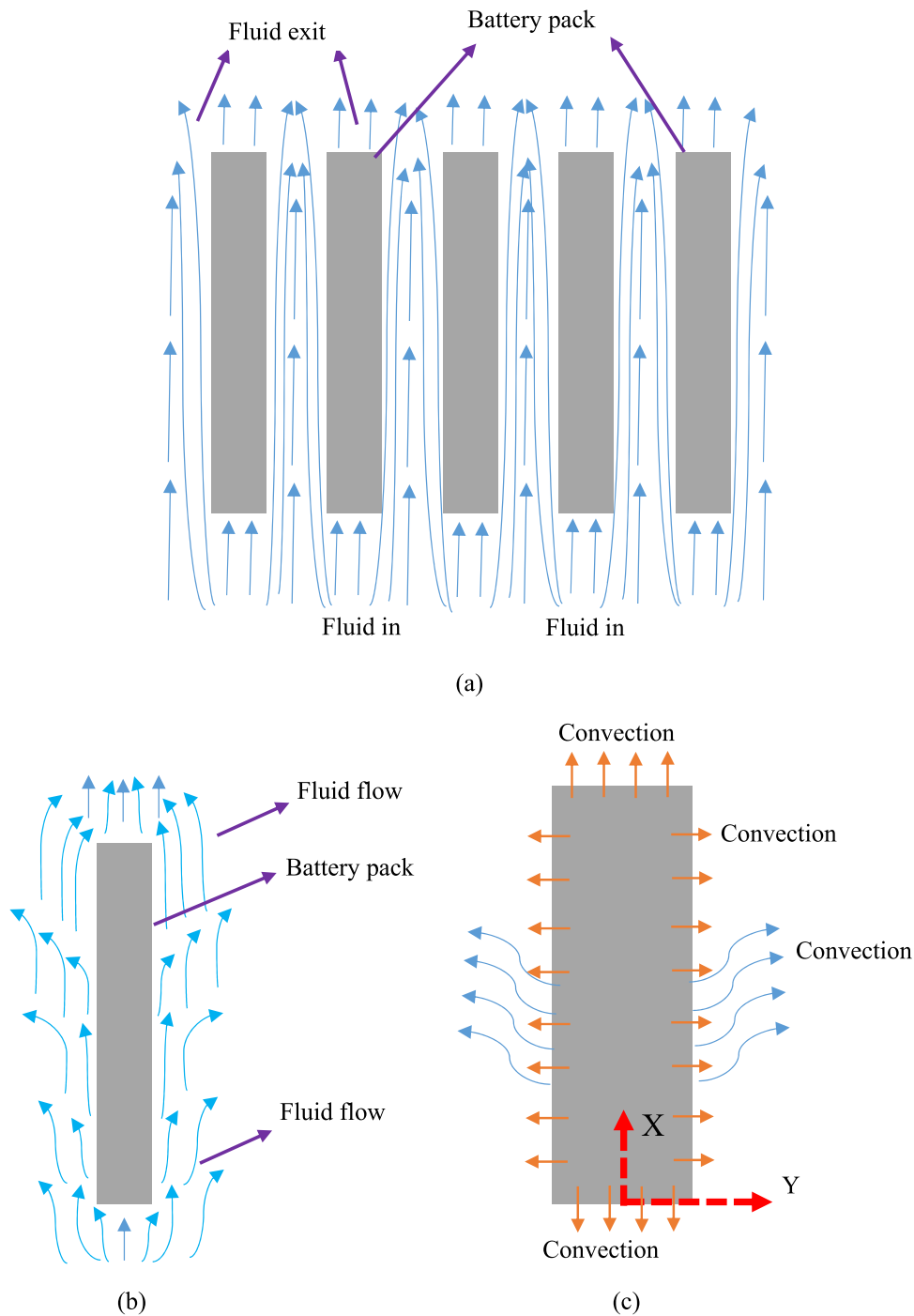


**Fig. 1** (a) Arrangement of battery packs cooled by coolant flow (b) battery pack with convection without considering the coolant.

domain are considered for evaluation. The direction of coolant flow is along the y-axis, as shown in Fig. 1. The convective heat transfer at the battery-coolant interface occurs as the coolant flows through the channels between the battery packs. The coolant flows at a low rate, maintains the laminar type of flow regime. The governing equations describing the heat transfer process when discharging/charging the Li-ion battery cell is given by

$$k_s \nabla^2 T + q''' = \rho c \frac{\partial T}{\partial t} \quad (1)$$

where  $q'''$  is the volumetric heat generation term.

In the first part of the study, only convection is considered at the boundary, as shown in Fig. 1 (b). During this, only the conduction Eq. (1) is solved. In the next section, coolant flow is considered, for which the following method is adopted.

For the conditions of two-dimensional, incompressible flow, laminar flow, steady and forced convective flow, the governing equations that define the computational model are continuity equation, momentum equations in  $x$  and  $y$ , and

energy equation. They are mathematically represented as follows:

$$\nabla \cdot u^* = 0 \quad (2)$$

$$\frac{\partial u^*}{\partial t} (u^* \cdot \nabla u^*) = -\frac{1}{\rho} \nabla p + \mu \nabla^2 u^* \quad (3)$$

$$\frac{\partial T^*}{\partial t} + u \cdot \nabla T^* = \frac{\alpha}{\rho c} \nabla^2 T^* \quad (4)$$

For computational simplicity, the normalizing parameters are non-dimensionalized. The set of non-dimensional parameters are as follows:

$$\begin{aligned} \bar{S}_q &= \frac{q''' w_s^2}{k_s (T_0 - T_\infty)}, C = 4Ar^2, \bar{T} = \frac{T - T_\infty}{T_0 - T_\infty}, L_i = \frac{L}{L}, L_o = \frac{L}{L} \\ X &= \frac{x}{L}, U = \frac{u}{u_\infty}, V = \frac{v}{u_\infty}, P = \frac{p}{\rho u_\infty^2}, A_r = \frac{L}{2w_s} \\ Y_s &= \frac{y_s}{w_s}, Y_f = 1 + \frac{y_f}{L}, \bar{W}_f = \frac{w_f}{L}, \zeta_{cc} = \frac{k_f}{k_s} \left[ \frac{w_s}{L} \right], \\ Re &= \frac{u_\infty L}{\nu}, Pr = \frac{\nu}{\alpha} \end{aligned} \quad (5)$$

The governing equations are non-dimensionalised, as given in the following equations:

$$\frac{\partial T_b}{\partial \tau} = \frac{\partial^2 T_b}{\partial X^2} + M \frac{\partial^2 T_b}{\partial Y_b^2} + MQ_{gen} \quad (6)$$

$$\nabla U = 0 \quad (7)$$

$$\frac{\partial U}{\partial \tau} + U \nabla U = -\nabla P + \frac{1}{Re} \nabla^2 U \quad (8)$$

$$\frac{\partial T_f}{\partial \tau} + U \nabla T_f = \frac{1}{Re Pr} \nabla^2 T_f \quad (9)$$

Appropriate boundary conditions are applied to solve the above governing flow and thermal equations. The relevant conditions to solve are presumed with an incoming  $T_\infty$  free stream temperature and velocity  $U_\infty$ . The top, bottom, right side, left side. Coupled condition at the interface is as follows:

The bottom convection condition and free stream velocity is

$$X = 0, 0 \leq Y_b \leq 1, k_b \frac{\partial T_b}{\partial Y_b} = h(T^* - T_\infty) \quad (10)$$

$$X = 0, 0 \leq Y_f \leq 1, U = 1, V = 0, T_f = 0 \quad (11)$$

As at the symmetrical left side, the domain is a mirror, the condition taken is

$$Y_b = 0, 0 \leq X \leq 1, \frac{\partial T_b}{\partial X} = 0 \quad (12)$$

At the top of the battery, the presence of current collectors dissipate heat by convection, hence

$$X = 1, 0 \leq Y_b \leq 1, -k_b \frac{\partial T_b}{\partial Y_b} = h(T^* - T_\infty) \quad (13)$$

Most importantly, the coupled condition at the interface is given by

$$Y_f = 0, 0 \leq X \leq L, \frac{\partial T_f}{\partial Y_f} = \frac{L}{W_b} \frac{1}{Cr} \frac{\partial T_b}{\partial Y_b}, U = 0, V = 0 \quad (14)$$

At the interface, continuity of temperature boundary conditions is used.

$$Y_b = 1, 0 \leq X \leq 1, T_b = T_f \quad (15)$$

When the fluid exits the channel with fully developed boundary condition,

$$X = L, 0 \leq Y_f \leq 1, \frac{\partial T_f}{\partial X} = 0, \frac{\partial U}{\partial Y_f} = 0, V = 0 \quad (16)$$

As only half of the domain is considered the internal channel flow, which is symmetric, the conditions for flow are

$$Y_f = W_f, 0 \leq X \leq L, \frac{\partial T_f}{\partial Y_f} = 0, V = 0, \frac{\partial U}{\partial Y_f} = 0 \quad (17)$$

### 2.1. Solution strategy and validation

Finite Volume Method (FVM) based staggered grid method is used to solve the energy and momentum equation of the conjugate heat transfer problem. The momentum in the x and y equation and continuity equation are simultaneously solved using the SIMPLE algorithm. The velocity and temperature governing equations are solved by a tri-diagonal matrix algorithm (TDMA). The equation of pressure change is solved using the Successive Over Relaxation (SOR) technique. The boundary conditions applied to maintain a brief presentation, the solution strategy, and the used numerical approaches are not specified in detail. A c-program (indigenous code) was developed to solve these governing equations and for the computational simulation. The developed code for the aforementioned mathematical formulation is validated with established works in literature. Richter et al. [30] studied the temperature profiles by experimenting on the thermal conductivity of the battery cells. Fig. 2 represents the temperature change with the heat generation rate obtained using the FVM code and similar previous research work results. They are in close conformity to each other.

### 3. Results and discussion

In the first part of the study, only the convection condition is adopted at the boundary; therefore, only the conduction Eq (1) with heat generation is solved. The temperature distribution and maximum temperature analysis in the battery are performed. In the next part, the conjugate condition at the battery and coolant interface is considered in Fig. 1 (a). The temperature distribution analysis is performed in the battery domain for various coolant flows.

Fig. 3 depicts the temperature behavior within the solid battery pack when  $Bi$  changes from 2 to 20. At the same time, other parameters like  $Re$ ,  $Pr$ ,  $Q_{gen}$ , and  $Cr$  of fluid and solid are kept constant. It is observed from the above Fig. 3 that with an increase in the  $Bi$ , the temperature in the battery pack decreases as it is known that with an increase in the  $Bi$ , the convection heat transfer coefficient increases, resulting in a drop in battery pack temperature. It is also observed that the temperature in the battery pack along its width remains constant concerning each  $Bi$ . For  $Bi$  of value 2, the temperature in the battery pack may reach the critical value, which may affect the thermal performance characteristics of the battery. At low  $Bi$ , the resistance to the convective mode of heat transfer is more, and resistance to conduction heat transfer is less; hence due to low conductance resistance, the temperature in

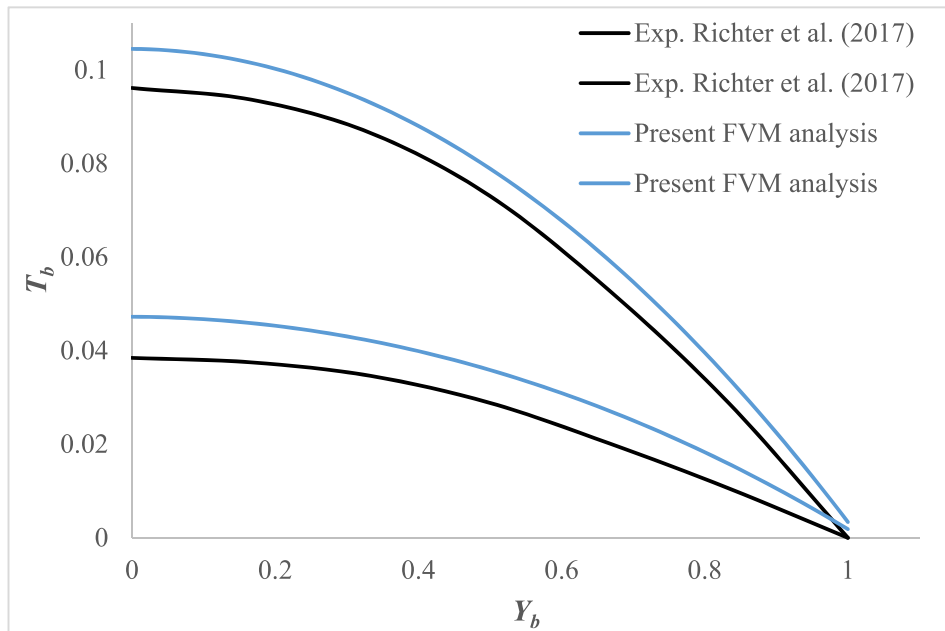


**Fig. 2** Validation of present FVM works with past experimental, analytical, and FEM analyses. In experimental work, the air is used as coolant fluid  $Pr = 0.7$ . The top two lines represent  $Q_{gen} = 0.2$ , and the lower two lines represent  $Q_{gen} = 0.1$ .

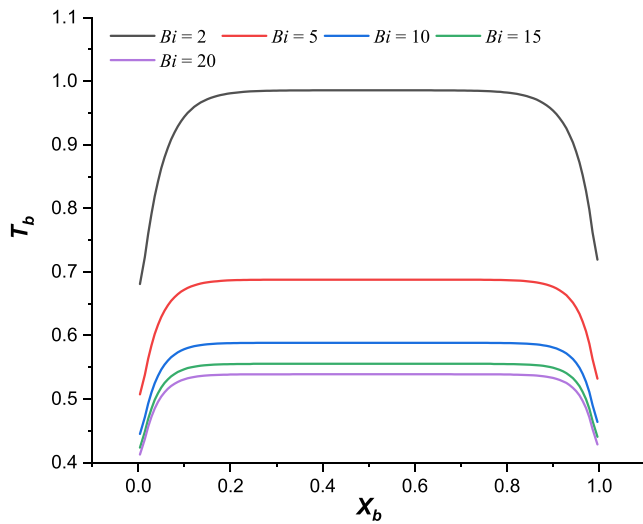


**Fig. 3** Biot number ( $Bi$ ) effect on the temperature of the battery.

the battery pack increases. But at  $Bi$  of 10 or above 10, the temperature drop within the battery pack is negligible; therefore, it is better to have a moderate range of  $Bi$  to achieve better battery thermal performance.

Fig. 4 illustrates the effect of total heat generation and  $Bi$  in a battery pack on its maximum temperature. It is observed from Fig. 4 that with an increase in heat generation, the maximum temperature in the battery pack increases. As the heat generation in the battery pack increases, it becomes challenging for the fluid to take away the heat from the battery; hence, the remaining heat energy makes the battery pack temperature rise. This rise in the maximum temperature in the battery pack

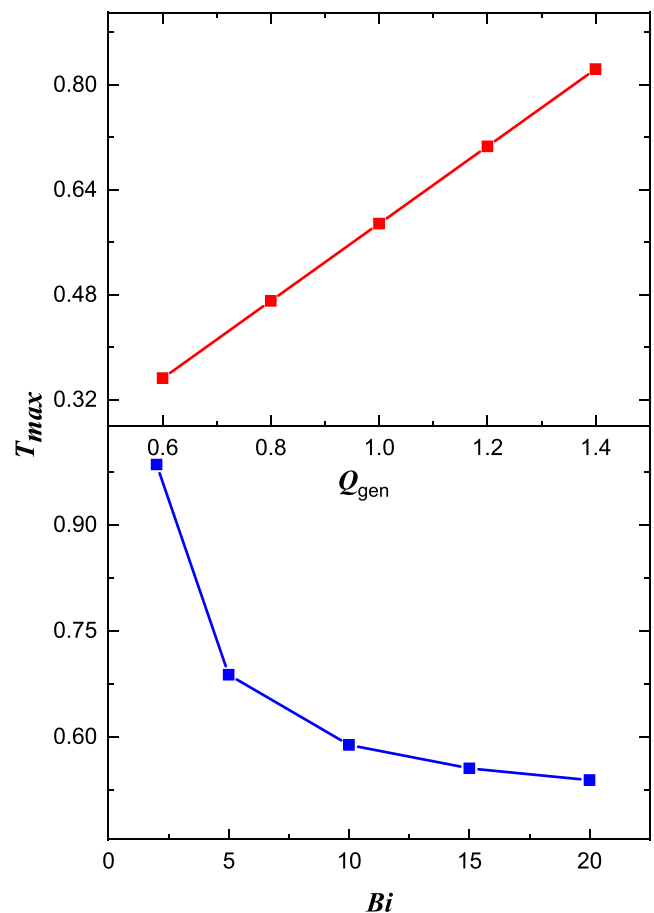


**Fig. 4** Maximum temperature with  $Bi$  and  $Q_{gen}$ .

has to be controlled to enhance the battery's performance characteristics. The rise in the maximum temperature of battery pack due volumetric heat generation may also be attributed to the fact that with a more significant amount of heat, the average kinetic energy level of the battery pack molecules increases to an extreme level which later may appear in the form of rising in the temperature. It is better to use appropriate heat generation in the battery pack to avoid overheating and thermal accidents in the battery pack system.

Fig. 2 shows that with the increase in the value of  $Bi$ , the maximum temperature in the battery pack decreases. Such behavior may be attributed to the fact that with the increase in the  $Bi$ , the resistance to heat transfer by conduction mode becomes strong. In contrast, resistance to the convection mode of heat transfer becomes weak, which may cause the fluid to carry more heat from the solid surface of the battery pack, leading to a decrease in the temperature in the battery pack. The  $Bi$  with a value of 2 may take the maximum temperature in the battery pack near the critical range above which the rise in the battery pack's temperature may partially or entirely terminate the thermal performance of the battery system. To have better battery life and high working efficiency of the battery system, it is always better to choose the safe range of  $Bi$ .  $Bi$  is also helpful in predicting the thermal conductivity of the solid battery; a higher range of  $Bi$  implies that the resistance to conduction mode of heat transfer is weak, and this weakness in the resistance appears in the form of better thermal conductivity of the solid battery pack.

Fig. 5 represents the effect of the heat generation parameter on the battery pack's temperature when the  $Bi$  is held constant. It is perceived from above Fig. 4 that with the increase in the heat generation within the battery pack, the temperature also increases. For  $Q_{gen} = 1.4$ , the temperature in the battery pack reaches near its upper limiting value. It is well established that when heat generation increases, the molecular activity within the battery pack increases, resulting in a corresponding increase in the kinetic energy that increases the battery pack's temperature. When the kinetic energy of the molecules within the battery pack increases, it results in random motion of

molecules that may tend to resist the flow of heat through the battery pack. This heat resistance will appear in the form of augmented temperature. Choosing the most suitable range of heat generation within the battery pack is mandatory to avoid the unnecessary rise in its temperature. It is good enough

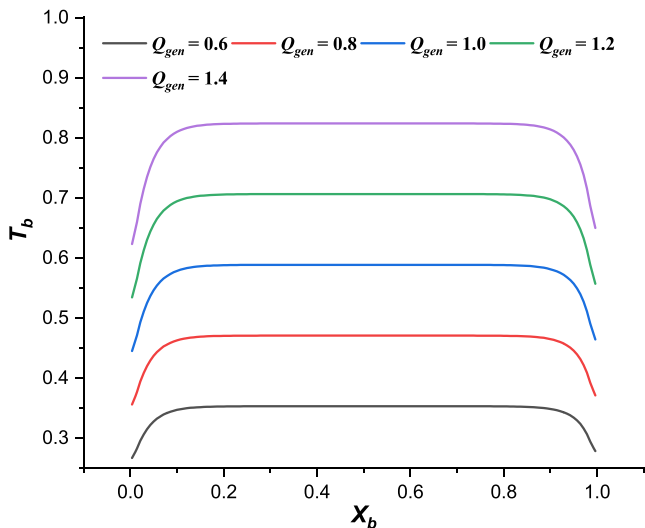
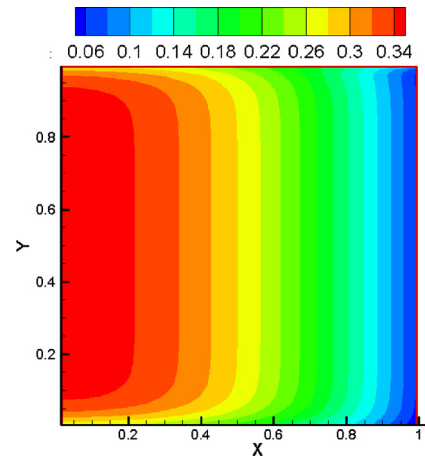
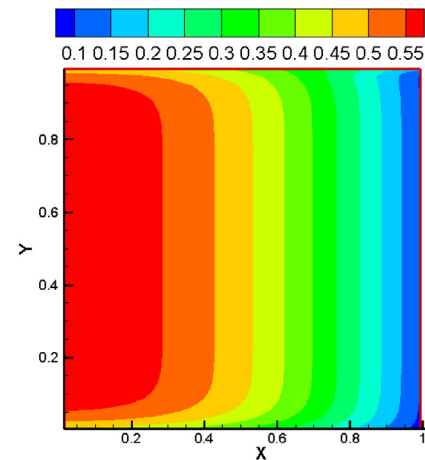


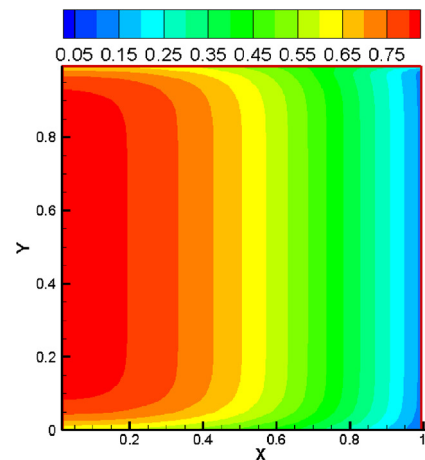
Fig. 5 Effect of  $Q_{gen}$  on battery temperate with convection from the surface.



(a)  $Q_{gen}=0.6$



(b)  $Q_{gen}=1.0$



(c)  $Q_{gen}=1.5$

Fig. 6 Temperature distribution in battery cell for  $Q_{gen}$ .

to have a moderate range of heat generation values to maintain better battery life and eliminate fire hazards and accidents.

Fig. 6 (a), (b), and (c) illustrate the temperature contour plots in the battery pack for the heat generation of 0.6, 1.0, and 1.5, respectively, while  $Bi$  is kept constant. It is observed from the above contours that with an increase in heat generation, the temperature within the battery pack also increases. As expected, it is a known fact that with an increase in heat generation, the resistance to heat transfer by conduction also increases, increasing the battery pack's temperature. It is also observed that the temperature in the transverse direction of the battery pack decreases irrespective of heat generation. It is known that with increase in the thickness of the battery pack, the thermal conductivity gets affected, which appears in the form of a drop in temperature. The contour region covered by the maximum temperature in the battery pack along the axial and transverse direction is more than the minimum temperature contour region in the battery pack. The temperature contours obtained for different heat generations in a battery pack suggest that high power density batteries usage may result in high-temperature zones, which may further cause the failure of the battery both in terms of thermal and structural aspects. Hence, it is best to have a moderate range of power densities to have more comprehensive thermal management of the battery system.

Richter et al. [47] and Dincer et al. [48] have investigated the ageing of battery cell and heat absorption characteristics of phase change materials used for cooling of battery cell. These studies have contributed similar temperature plots for varying C-rates in the transverse direction of the cell. The axial temperature noted  $\Delta T = 1.22$ , conversely the surface temperature  $\Delta T_s = 0.75$ . This temperature gradient is established as a result of convection heat transfer initiated by the coolant flowing over the cell wall surface. It is also evident that at higher  $Q_{gen}$  the thermal gradient is considerable and at lower  $Q_{gen}$  the thermal gradient is negligible. Thus lumped model can be considered at lower  $Q_{gen}$  for the analysis as reported by Huang et al. [49] and few others [50–52].

Fig. 6 manifests that with enhancement of  $Q_{gen}$  the axial temperature attains a peak value and further rise will cross the threshold temperature ( $T_o$ ), causing thermal runaway. This critical temperature can cause oxidation at the cathode, which in turn if reacts with the electrolyte catches fire. Thermal runaway degrades the battery performance, causes electrolyte leakage, loss of shelf life, detonation etc., [53–55]. Hence, the volumetric heat generation must be within operational limits. This can be achieved by controlled charging and discharging, selection of efficient cooling system, hybrid mode utilization under peak load conditions etc., [56]. Increasing the coolant flow velocity can lower the temperature but the energy requirement to run a fan develops. Thus, the influence of  $Re$  on the battery thermal behavior is important factor in a cooling mechanism.

Fig. 7 (a), (b), and (c) depicts the temperature contours of the battery pack for various  $Bi$ . At the same time, the  $Re$ ,  $Pr$ ,  $Cr$ , and  $Q_{gen}$  parameters are kept constant, as it is evident from the Figure, with an increase in the  $Bi$ , the temperature within the battery pack decreases. This behavior is mainly due to an increase in the convection heat transfer from the surface of the battery to the surrounding fluid medium, as the higher value of  $Bi$  implies the higher resistance to conduction heat transfer. It is also observed that the region covered by

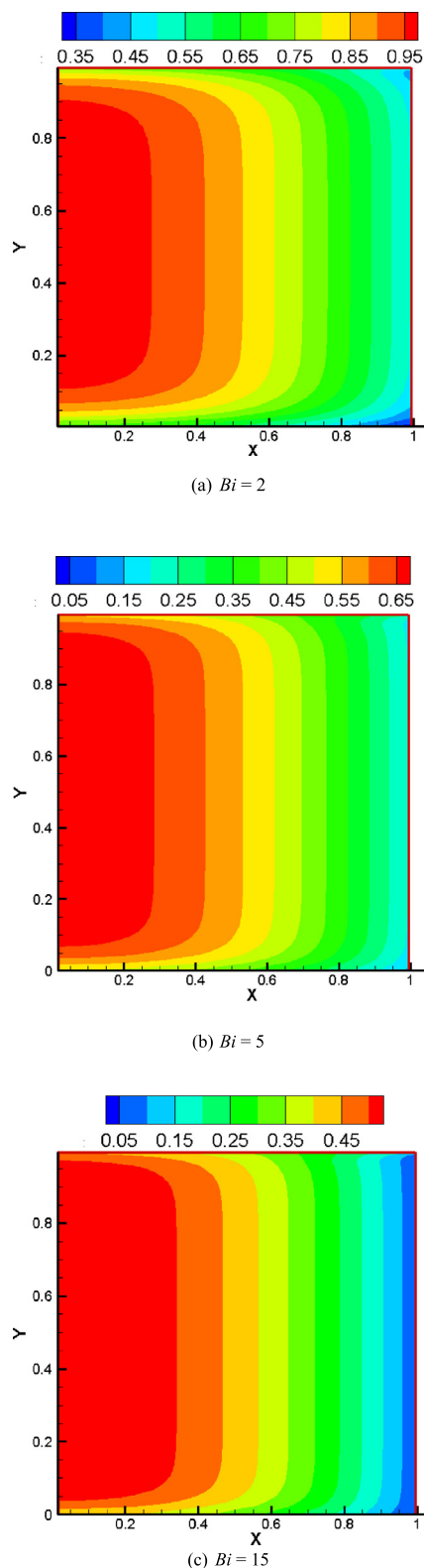


Fig. 7 Temperature distribution in battery cell for  $Bi$ .

the maximum and minimum temperature contour zones coverage space in the battery pack is more in the axial direction than the transverse direction. Such temperature contours pattern indicates that the thermal diffusivity is dominant in the axial

direction. It is also observed that for the low value of  $Bi$ , the chances of temperature rise in the battery pack above the critical limit are more as the resistance to heat transfer by convection mode dominates the heat transfer by conduction mode. It is necessary to have a suitable range of  $Bi$  to maintain the temperature limit in the battery pack within the safe limit.

In the following part, the conjugate condition, i.e., continuity of heat flux and temperature at the coolant and pack interface, is adopted, and the effect of  $Pr$  is analyzed. Fig. 8 illustrates the temperature contours in a battery pack when air is used as a coolant while the  $Re$ ,  $Q_{gen}$ , and  $Cr$  are constant. As observed in Fig. 8, the maximum temperature region in a battery is shifted towards the vicinity of its trailing end. It is also seen that the temperature in the battery pack crosses its safer limit value which may result in its meltdown. Since air, when used as a coolant having poor thermal conductivity, may carry only a limited amount of heat, the residual of heat will appear in the form of temperature rise, observed in the above Fig. 8. Since the maximum temperature regions located at the trailing edge of the battery pack result in the uneven thermal expansion of the battery, which further results in fire accidents. Therefore, to enhance the performance of the battery system, it is necessary to have a better coolant that can control the rise in temperature of the battery by carrying a good amount of heat under conjugate conduction–convection conditions. When air is used as a coolant, it is better to reduce the battery pack's power density or increase the flow velocity of the air, which further increases the pumping cost. Finally, it is also seen that the critical temperature region occupies the maximum space in the battery pack, i.e., the temperature equal and above 1. Such temperature distribution within the battery pack creates maximum chances of fire hazards.

Fig. 9 illustrates the temperature contours under conjugate heat transfer for battery pack subjected to flow of water when the parameters like  $Re$ ,  $Cr$ , and  $Q_{gen}$  are kept at their base value. From the close observation of above Fig. 9, it can be said that when water is used as a coolant, the temperature in the battery pack can be controlled well within the safe limit. The temperature of the battery pack is decreasing in the transverse direction. It reaches its minimum value at the lateral surface of the battery pack, where the fluid comes in contact with it. Water can be a better choice for coolant. Still, its high den-

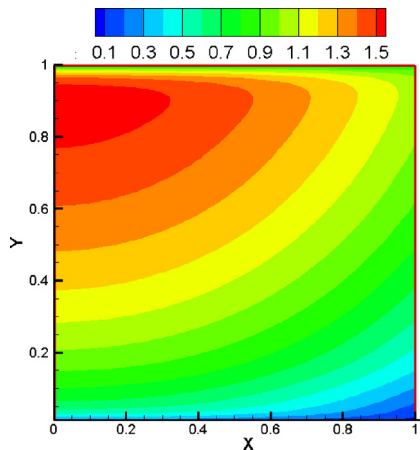


**Fig. 8** Temperature contours in battery pack when  $Pr = 0.7$  (Air).

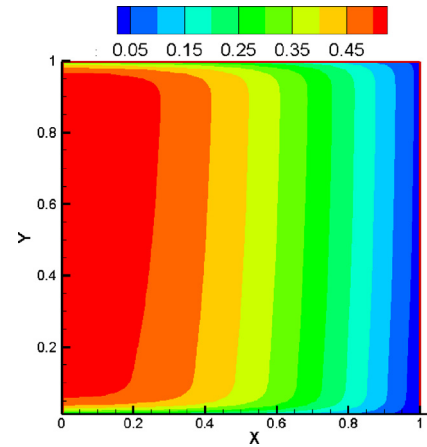


**Fig. 9** Temperature contours in battery pack when  $Pr = 6.9$  (Water).

sity and viscosity compared to air need more pumping power, increasing the overall cost of a battery thermal management system. When the power density of the battery pack is taken into consideration, the water as a coolant replaces the air due to its good thermal properties. The convection coefficient is high in the water, which plays a vital role in the conjugate heat transfer process. The battery thermal accidents and fire hazard chances can be reduced to a greater extent by using water as a coolant.

Fig. 10 depicts the temperature contours in a battery pack when subjected to the flow of dielectric oil, which will act as a coolant, whereas the parameters  $Re$ ,  $Cr$ ,  $Q_{gen}$ , and  $Bi$  are kept constant. One can easily predict from the temperature contours, as shown in Fig. 3, that using dielectric oil as a coolant can control the temperature in the battery pack in a permissible limit. From the temperature contours, it is seen that when the coolant enters at the leading edge of the battery pack, it carries the maximum amount of heat. But as the coolant further flows downstream, its ability to carry the heat decreases. Hence, such behavior of the coolant makes the battery pack's temperature rise at the trailing end. Since the dielectric oil has more viscosity, it makes it difficult to pump and tends to create

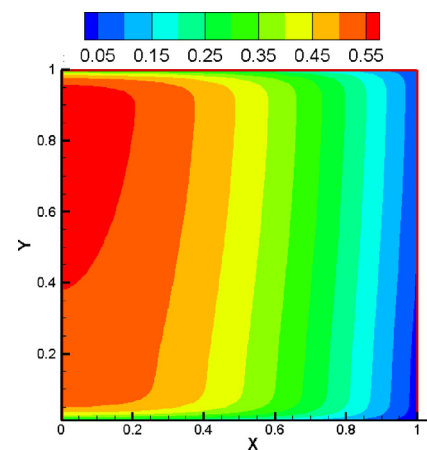


**Fig. 10** Temperature Contours in battery pack  $Pr = 21.7$  (Dielectric oil).

a thick velocity boundary layer, which further makes it a poor heat conductor. As dielectric oils are more prone to catch fire even at low temperatures, one should consider the fire hazards while using dielectric oil as a coolant.

The effect of silicone thermal oil on the temperature contours of the battery pack as a coolant in the battery cooling system is depicted in Fig. 11, where the parameters like  $Re$ ,  $Bi$ ,  $Cr$ , and  $Q_{gen}$  are held at their base values. As the Syltherm 800 has good heat transfer characteristics, it can maintain the temperature in the battery pack in a well-defined safe limit. The temperature contours of Fig. 11 depict that the heat dissipation from the battery pack to the surrounding coolant is at a uniform rate. Hence, the Syltherm fluids prove to be a good choice for the cooling system of the batteries since Syltherm fluids are costly but have low viscosity, affecting the velocity and thermal boundary layer at the battery coolant interface. The low viscosity of these oils also results in low pumping power. Syltherm oil may be a good choice as a coolant but with a high cost. As the temperature contour shows uniform space occupancy, the heat transfer rate also remains uniform, which will improve battery life.

Fig. 12 shows the temperature contours obtained in a battery pack under conjugate conduction-convection condition subjected to flow of a coolant having a Prandtl number of 0.0303. At the same time, the parameters  $Re$ ,  $Cr$ ,  $Q_{gen}$ , and  $Bi$  are held constant. When GaIn20 is used as a coolant due to its excellent thermal conductivity compared to water, it will transfer more heat from the surface of the battery pack. But the temperature distribution pattern in the battery pack says that the heat transfer from the lateral surface of the battery to the surrounding coolant is not uniform. The uneven temperature distribution pattern also predicts that the battery's performance is greatly influenced as such a temperature pattern could cause thermal stresses, which further deteriorate the battery structure. Hence one should be very careful while selecting the most proper coolant, which can improve the thermal performance of the battery.

The behavior of temperature in the battery pack subjected to flow of water with a ratio of conductivity between fluid and solid domain as 0.1 and other parameters such as  $Re$ ,  $Pr$ ,  $Q_{gen}$ , and  $Bi$  are kept constant. From the temperature contours, it can be said that when the conductivity ratio between

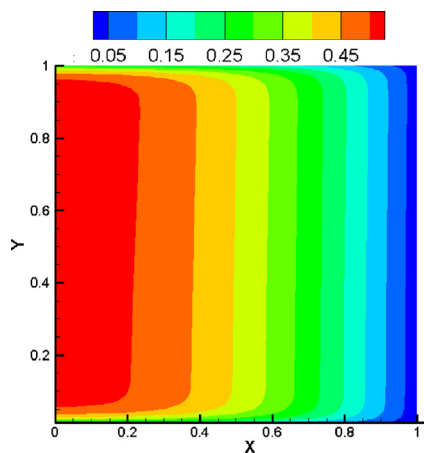


Fig. 11 Temperature Contours in battery pack  $Pr = 101.5$  (Syltherm 800).

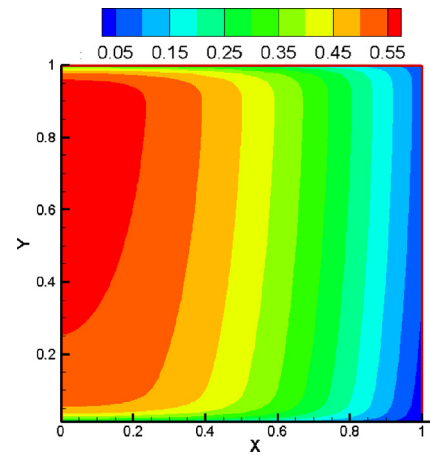


Fig. 12 Temperature Contours in battery pack for  $Pr = 0.0303$  (GaIn<sup>20</sup>).

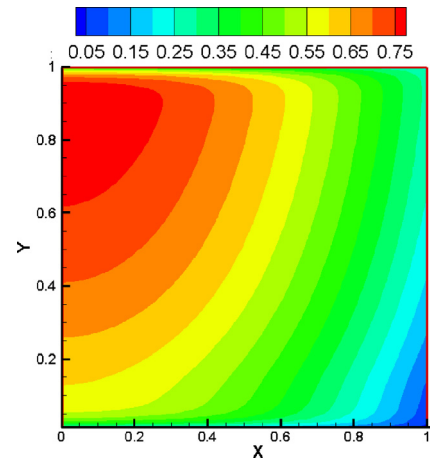
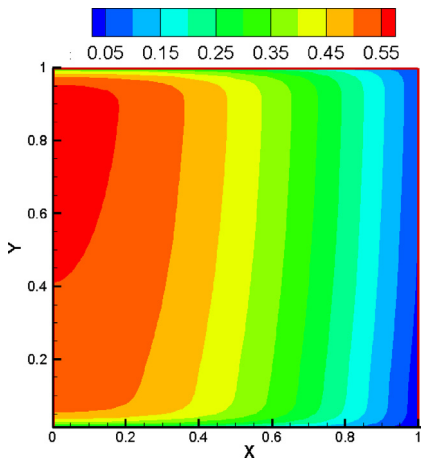


Fig. 13 Temperature contour in battery pack when  $Cr = 0.1$  (Water).

the coolant and battery pack is kept at a value of 0.1, the distribution of heat in the battery is not uniform, which results in a non-uniform temperature affecting the overall performance of the battery. It is also observed from Fig. 13 that the maximum temperature contours are located near the top end of the battery. In contrast, at the bottom end, the temperature of the battery is low. Such high and low-temperature regions in the battery pack create uneven thermal stresses, resulting in battery failure. To have better performance results for the battery system, one should maintain the proper balance of thermal conductivity between the solid and fluid domains.

Figs. 14, 15, 16, and 17 illustrate the effect of  $Cr$  on the temperature contours of the battery when subjected to the flow of coolant with the coupled conduction-convection condition. The parameters  $Re$ ,  $Q_{gen}$ , and  $Pr$ , are retained at their predefined value. It can be said from the above temperature contours that with the increase in the conductivity ratio between the coolant and battery, the temperature in the battery pack decreases up to a value of  $Cr = 1.0$ , beyond which the temperature increases. It is a known fact that with an increase in the conductivity ratio, the thermal conductivity of the coolant increases, which further decreases the temperature in the bat-



**Fig. 14** Temperature contours in battery pack when  $Cr = 0.5$  (Water).

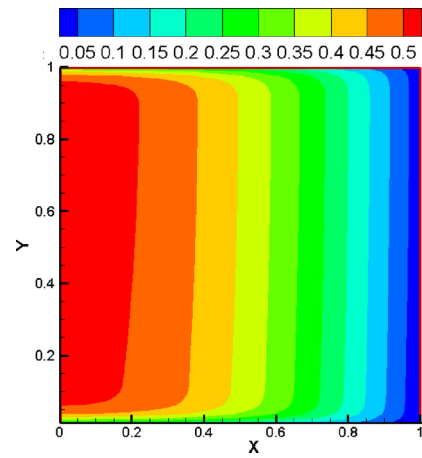


**Fig. 17** Temperature contours in battery pack when  $Cr = 2.0$  (Water).

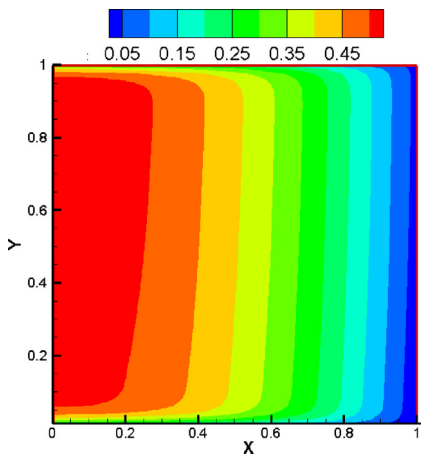


**Fig. 15** Temperature contours in battery pack when  $Cr = 1.0$  (Water).

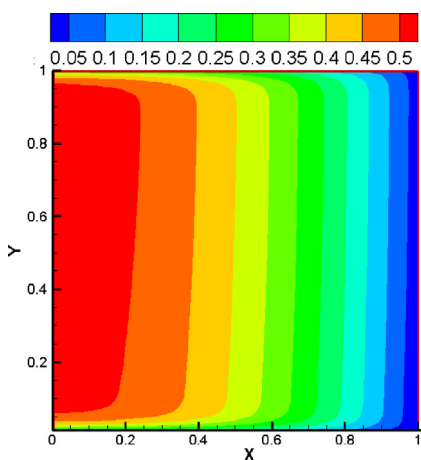


**Fig. 16** Temperature contours in battery pack when  $Cr = 1.5$  (Water).

tery pack. Figs. 7, 8, 9, and 10 show a critical value of conductivity ratio ( $Cr = 1.0$ ) above which the temperature in the bat-

tery once again increases. Hence one should make use of the appropriate value of conductivity ratio between coolant and battery. The temperature distribution in the battery becomes more uniform with an increase in the conductivity ratio, which is seen in the temperature contour plots. The uniform distribution of temperature is essential for the better and improved performance of the battery system. At higher values of the  $Cr$ , the heat dissipation from the battery to the coolant becomes more uniform, which further makes the coolant carry more heat. When water is used as a coolant in the thermal management of the battery pack, it is advisable to use a balanced ratio of thermal conductivity between the fluid and solid domain. Both efficiency and life of the battery can be improved to a greater extent by using suitable selected thermal parameters.

Figs. 18–22 illustrate the temperature contours in a battery pack subjected to airflow at different Reynolds numbers. It is observed from Fig. 18 that at Reynolds number of 100, the temperature at the bottom leading edge of the battery temperature remains low, this is due to convection boundary condition, and the fluid enters with its free stream temperature. As we move along the height of the battery pack, the temperature

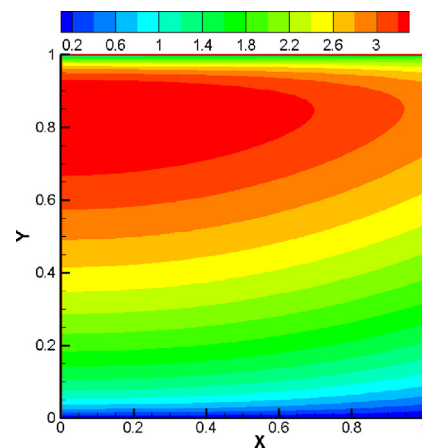


**Fig. 18** Temperature contour of the battery pack at  $Re = 100$  (air).

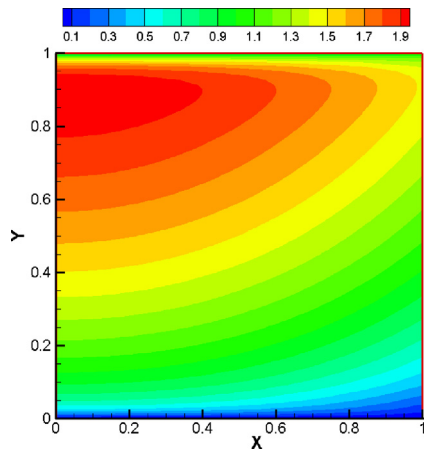


**Fig. 19** Temperature contour of the battery pack at  $Re = 500$  (air).

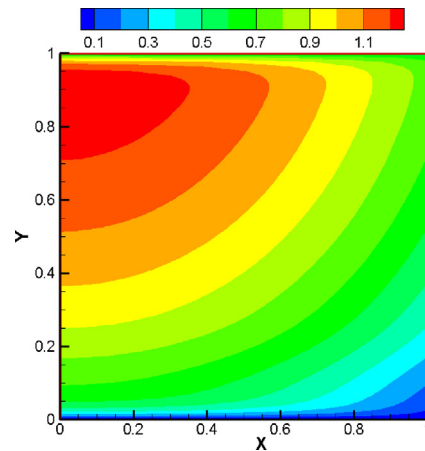


**Fig. 22** Temperature contour of the battery pack at  $Re = 2000$  (air).

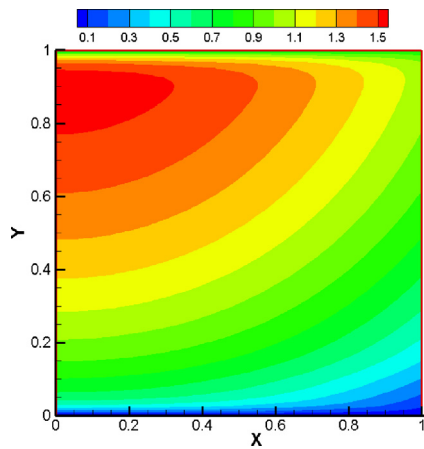


**Fig. 20** Temperature contour of the battery pack at  $Re = 1000$  (air).

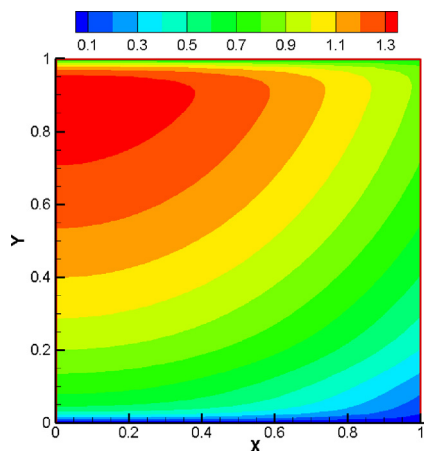


**Fig. 21** Temperature contour of the battery pack at  $Re = 1500$  (air).

increases, and ample space is covered by the high-temperature regions at the top end of the battery at the height of 0.7 to 0.9

along the Y direction. But again, the drop in temperature can be seen due to the convection boundary condition at the top surface of the battery pack. The range of temperature within the battery pack is very high due to the low convective heat transfer coefficient as the Reynolds number is low. The chance of building up Thermal stresses are very high at a low Reynolds number since the maximum temperature contour space is more which may tend to reduce the thermal diffusivity across the battery surface. Hence high-temperature spots were built up, leading to cross the maximum temperature beyond the safe limit.

The behavior of all the above plotted temperature contours for other Reynolds number values of 500, 1000, 1500, and 2000, as shown in Figs. 19–22, are identical. Still, the temperature within the battery pack gets reduced with an increase in the Reynolds number. Even the space occupied by the maximum temperature contours decreases, which tends to improve the thermal diffusivity from the battery surface. Hence the chances of overheating or thermal stresses are very much reduced at high Reynolds numbers. It is also observed that irrespective of Reynolds number, the maximum temperature contour on the battery surface remains near the top end of the battery pack. The low-temperature contour regions at the bottom of the battery pack are drifting towards the right side of the battery pack along with X and Y coordinates. It is also observed that the uniformity in temperature distribution on the battery pack increases with the increase in the Reynolds number. The uniform temperature distribution is a good sign for the improvement in the thermal performance of batteries.

The temperature difference noticed at elevated values  $Re$  is less. This is because only a considerable heat dissipation can be secured from the cell surface. These findings were reported by Mahamud and Park [57] and Tong et al. [58]. This emphasis that extensive increment of  $Re$  would not bring efficient cooling but will add to the energy demands of fan operation required for air circulation. It can be observed that maximum temperature difference  $\Delta T_{max}$  is higher at  $Re = 1000$  and  $Re = 250$  contrary to that at  $Re = 750$  and  $Re = 2000$ . Rao et al. [57] and Tong et al. [58] have synthesized a relevant trend in  $T_{max}$  variation at higher air flow velocities. Thus it can be concluded that for considerable range of  $Q_{gen}$  the  $Re \leq 1000$

is not recommendable as the peak temperature surpasses the threshold limit [59].

#### 4. Conclusion

The numerical analysis of heat transfer from a battery pack is carried out considering conjugate and non-conjugate conditions. FVM based code is written, and validation is performed with experimental work. The effect of Biot number, heat generation, Prandtl number, and conductivity ratio is performed. The following conclusions are derived from the in detail numerical analysis:

1. In non-conjugate analysis, the temperature gradients are sharp and similar profiles are at the top and bottom of the battery. The temperature distribution is found to be uniform in the non-conjugate analysis where the flow of coolant flow consideration is not considered.
2. The conjugate analysis reveals that the temperature distribution is non-uniform at the top and bottom of the battery. The maximum temperature of battery pack is located at the top portion of the battery where the electrodes are placed. Temperature of pack is low at the bottom surface due to direct contact of the coolant which comes in contact as fresh.
3. When air is considered as the coolant in conjugate condition, the maximum temperature is very high and crosses the critical limit in the battery. With water as coolant; the maximum temperature at the temperature at the pack and coolant interface is low. The temperature distribution resembles that of non-conjugate conditions when water is employed.
4. Increasing the conductivity ratio shows that the temperature drops in the battery significantly. It is better to choose a suitable fluid and conductivity ratio for the safe operation of the battery.
5. The regions with high and low temperatures at the top and bottom of the battery pack produces uneven thermal stress, later causing the failure of the battery. Choosing an appropriate range of thermal conductivity ratio that balances the solid and the fluid field to get better battery system performance results is required.

#### Declaration of Competing Interest

The authors declare that they have no known competing financial interests or personal relationships that could have appeared to influence the work reported in this paper.

#### Acknowledgement

The authors extend their appreciation to the Deanship of Scientific Research at King Khalid University, Saudi Arabia for funding this work through Research Group Program under Grant No: R.G.P.1/104/42. Authors would like to express their gratitude to the United Arab Emirates University, Al Ain, UAE for providing the financial support with Grant No. 12S086.

#### References

- [1] Hossein Maleki, Said Al Hallaj, J. Robert Selman, Ralph B. Dinwiddie, H. Wang, Thermal Properties of Lithium-Ion Battery and Components, 1999.
- [2] T.D. Hatchard, D.D. MacNeil, A. Basu, J.R. Dahn, Thermal Model of Cylindrical and Prismatic Lithium-Ion Cells, 2001.
- [3] Gi-Heon Kim, Ahmad Pesaran, Robert Spotnitz, A three-dimensional thermal abuse model for lithium-Ion cells, 2007.
- [4] Guifang Guo, Bo Long, Bo Cheng, Shiqiong Zhou, Peng Xu, Binggang Cao, Three-dimensional thermal finite element modeling of lithium-ion battery in thermal abuse application, 2010.
- [5] Rajib Mahamud, Chanwoo Park, Reciprocating airflow for Li-ion battery thermal management to improve temperature uniformity, 2011.
- [6] G. Karimi, A.R. Dehghan, Thermal Management Analysis of a Lithium-Ion Battery Pack using Flow Network Approach, 2012.
- [7] G. Karimi, X. Li, Thermal management of lithium-ion batteries for electric vehicles, 2012.
- [8] Ahmadou Samba, Noshin Omar, Hamid Gualous, Peter Van den Bossche, Joeri Van Mierlo, Tala Ighil Boubekeur, Development of 2D Thermal Battery Model for Lithium-ion Pouch Cells, 2013.
- [9] O.S. Burheim, M.A. Onsrud, J.G. Pharoah, F. Vullum-Bruer, P. J.S. Vie, Thermal Conductivity, Heat Sources and Temperature Profiles of Li-Ion Secondary Batteries, 2013.
- [10] Heesung Park, A design of airflow configuration for cooling lithium-ion battery in hybrid electric vehicles, 2013.
- [11] Kuan-Cheng Chiu, Chi-Hao Lin, Sheng-Fa Yeh, Yu-Han Lin, Kuo-Ching Chen, An electrochemical modeling of lithium-ion battery nail penetration, 2014.
- [12] Yong Seok Choi, Dal Mo Kang, Prediction of thermal behaviors of an air-cooled lithium-ion battery system for hybrid electric vehicles, 2014.
- [13] S.J. Drake, D.A. Wetz, J.K. Ostanek, S.P. Miller, J.M. Heinzl, A. Jain, Measurement of anisotropic thermophysical properties of cylindrical Li-ion cells, 2014.
- [14] Yutao Huo, Zhonghao Rao, Xinjian Liu, Jiateng Zhao, Investigation of power battery thermal management by using the mini-channel cold plate, 2015.
- [15] N. Javani, I. Dincer, G.F. Naterer, G.L. Rohrauer, Modeling of passive thermal management for Electric vehicle battery packs with PCM between cells, 2014.
- [16] S. Panchal, I. Dincer, M. Agelin-Chaab, R. Fraser, M. Fowler, Experimental and theoretical investigations of heat generation rates for a water-cooled LiFePO<sub>4</sub> battery, 2016.
- [17] Divya Chalise, Krishna Shah, Ravi Prasher, Ankur Jain, Conjugate heat transfer analysis of thermal management of a Li-ion battery pack, 2017.
- [18] Xuning Feng, Minggao Ouyang, Xiang Liu, Languang Lu, Yong Xia, Xiangming He, Thermal runaway mechanism of lithium-ion battery for electric vehicles: A review, 2018.
- [19] Ke Li, Jiajia Yan, Haodong Chen, Qingsong Wang, Water cooling based strategy for lithium-ion battery pack dynamic cycling for a thermal management system, 2017.
- [20] Liwen Zhang, Peng Zhao, Meng Xu, Xia Wang, Computational identification of the safety regime of Li-ion battery thermal runaway, 2018.
- [21] Asif Afzal, Imran Mokashi, Sher Afghan Khan, Nur Azam Abdullah, Muhammad Hanafi Bin Azami, Optimization and analysis of maximum temperature in a battery pack affected by low to high Prandtl number coolants using response surface methodology and particle swarm optimization algorithm, Numer. Heat Transf. Part A Appl. 79 (5) (2021) 406–435, <https://doi.org/10.1080/10407782.2020.1845560>.

- [22] A. Afzal, A. Abidi, A. Samee, R. Razak, M. Soudagar, A. Saleel, Effect of parameters on the thermal and fluid flow behavior of battery thermal management system, *Therm. Sci.* (2020) 290, <https://doi.org/10.2298/tsci191206290a>.
- [23] I. Mokashi, S. Afghan, A. Nur, B. Hanafi Abdullah, Muhammad Azami, A. Afzal, Maximum temperature analysis in a Li-ion battery pack cooled by different fluids, *J. Therm. Anal. Calorim.* (2020) 1–17, <https://doi.org/10.1007/s10973-020-10063-9>.
- [24] A. Afzal, Z. Ansari, M.K. Ramis, Parallel performance analysis of coupled heat and fluid flow in parallel plate channel using CUDA, *Comput. Appl. Math.* 39 (2020) 219, <https://doi.org/10.1007/s40314-020-01244-1>.
- [25] Asif Afzal, Zahid Ansari, M.K. Ramis, Parallelization of Numerical Conjugate Heat Transfer Analysis in Parallel Plate Channel Using OpenMP, *Arab. J. Sci. Eng.* 45 (11) (2020) 8981–8997, <https://doi.org/10.1007/s13369-020-04640-1>.
- [26] Asif Afzal, A.D. Mohammed Samee, R.K. Abdul Razak, M.K. Ramis, Thermal management of modern electric vehicle battery systems (MEVBS), *J. Therm. Anal. Calorim.* 144 (4) (2021) 1271–1285, <https://doi.org/10.1007/s10973-020-09606-x>.
- [27] A. Afzal, A.D. Mohammed Samee, R.K. Abdul Razak, M.K. Ramis, Effect of spacing on thermal performance characteristics of Li-ion battery cells, *J. Therm. Anal. Calorim.* 135 (3) (2019) 1797–1811, <https://doi.org/10.1007/s10973-018-7664-2>.
- [28] R. Pinto, A. Afzal, L. D'Souza, Z. Ansari, A.D. Mohammed Samee, Computational Fluid Dynamics in Turbomachinery: A Review of State of the Art, *Arch. Comput. Methods Eng.* 24 (3) (2017) 467–479, <https://doi.org/10.1007/s1183>.
- [29] A. Afzal, Z. Ansari, A. Faizabadi, M. Ramis, Parallelization strategies for computational fluid dynamics software: state of the art review, *Arch. Comput. Methods Eng.* 24 (2) (2017) 337–363, <https://doi.org/10.1007/s11831-016-9165-4>.
- [30] Frank Richter, Signe Kjelstrup, Preben J.S. Vie, Odne S. Burheim, Thermal conductivity and internal temperature profiles of Li-ion secondary batteries, *J. Power Sources* 359 (2017) 592–600.
- [31] I. Mahariq, A. Erciyas, A spectral element method for the solution of magnetostatic fields, *Turk J Elec Eng & Comp Sci* 25 (2017) 2922–2932, <https://doi.org/10.3906/elk-1605-6>.
- [32] H. Kurt, M. Kuzuoglu, Questioning Degree of Accuracy Offered by the Spectral Element Method in Computational Electromagnetics, *ACES J.* 30 (7) (July 2015).
- [33] I. Mahariq, M. Kuzuoglu, I.H. Tarman, H. Kurt, Photonic Nanojet Analysis by Spectral Element Method, *IEEE Photonics J.* 6 (5) (2014) 1–14, <https://doi.org/10.1109/JPHOT.2014.2361615>.
- [34] M. Kuzuoglu, H. Tarman, On the Attenuation of the Perfectly Matched Layer in Electromagnetic Scattering Problems with the Spectral Element Method, *ACES Journal* 29 (9) (September 2014).
- [35] I. Mahariq, On the application of the spectral element method in electromagnetic problems involving domain decomposition, *Turk. J. Elec. Eng. Comp. Sci.* 25 (2017) 1059–1069, <https://doi.org/10.3906/elk-1511-115>.
- [36] Muhammad Sohail, Rahila Naz, Zahir Shah, Poom Kumam, Phatiphat Thounthong, Exploration of temperature dependent thermophysical characteristics of yield exhibiting non-Newtonian fluid flow under gyrotactic microorganisms, *AIP Adv.* 9 (12) (2019) 125016, <https://doi.org/10.1063/1.5118929>.
- [37] Muhammad Sohail, Rahila Naz, Sara I. Abdelsalam, Application of non-Fourier double diffusions theories to the boundary-layer flow of a yield stress exhibiting fluid model, *Phys. A* 537 (2020) 122753, <https://doi.org/10.1016/j.physa.2019.122753>.
- [38] M. Sohail, R. Naz, S.I. Abdelsalam, On the onset of entropy generation for a nanofluid with thermal radiation and gyrotactic microorganisms through 3D flows, *PHYSSCR-108549.R1*. <https://doi.org/10.1088/1402-4896/ab3c3f>.
- [39] Muhammad Sohail, Rahila Naz, Modified heat and mass transmission models in the magneto hydrodynamic flow of Sutterby nanofluid in stretching cylinder, *Phys. A* 549 (2020) 124088, <https://doi.org/10.1016/j.physa.2019.124088>.
- [40] R. Naz, S. Tariq, M. Sohail, Z. Shah, Investigation of entropy generation in stratified MHD Carreau nanofluid with gyrotactic microorganisms under Von Neumann similarity transformations, *Eur. Phys. J. Plus* 135 (2020) 178, <https://doi.org/10.1140/epjp/s13360-019-00069-0>.
- [41] S. Bilal, Heat transport in the convective Casson fluid flow with homogeneous-heterogeneous reactions in Darcy-Forchheimer medium, *Multidiscip. Model. Mater. Struct.* 15 (6) (2019) 1170–1189, <https://doi.org/10.1108/MMMS-11-2018-0202>, pp. 1573–6105.
- [42] M. Ghalandari, H. F. Fard, A. K. Birjandi, I. Mahariq, Energy related carbon dioxide emission forecasting of four European countries by employing data driven methods, *J. Therm. Anal. Calorimet.* <https://doi.org/10.1007/s10973-020-10400-y>.
- [43] A. Shafiq, T.N. Sindhu, Q.M. Al-Mdallal, A sensitivity study on carbon nanotubes significance in Darcy-Forchheimer flow towards a rotating disk by response surface methodology, *Sci. Rep.* 11 (2021) 8812, <https://doi.org/10.1038/s41598-021-87956-8>.
- [44] Anum Shafiq, Tabassum Naz Sindhu, Chaudry Masood Khalique, Numerical investigation and sensitivity analysis on bioconvective tangent hyperbolic nanofluid flow towards stretching surface by response surface methodology, *Alexand. Eng. J.* 59 (6) (2020) 4533–4548, <https://doi.org/10.1016/j.aej.2020.08.007>.
- [45] S. Anum, M. Oudina, Fateh, S. T. Naz, A. Awatef, A study of dual stratification on stagnation point Walters' B nanofluid flow via radiative Riga plate: a statistical approach, *Eur. Phys. J Plus* 136(4) (article id.407). <http://dx.doi.org/10.1140/epjp/s13360-021-01394-z>.
- [46] A. Shafiq, Z. Hammouch, T.N. Sindhu, D. Baleanu, Statistical Approach of Mixed Convective Flow of Third-Grade Fluid towards an Exponentially Stretching Surface with Convective Boundary Condition, *Special Functions and Analysis of Differential Equations*, first ed., 2020 (Pages 13, eBook ISBN 9780429320026).
- [47] F. Richter, P.J.S. Vie, S. Kjelstrup, O.S. Burheim, Measurements of ageing and thermal conductivity in a secondary NMC-hard carbon Li-ion battery and the impact on internal temperature profiles, *Electrochim. Acta* 250 (2017) 228–237, <https://doi.org/10.1016/j.electacta.2017.07.173>.
- [48] I. Dincer, H. Hamut, N. Javani, Thermal management of electric vehicle battery systems, John Wiley & Sons Ltd, 2017, <https://doi.org/10.1002/9781118900239>.
- [49] P. Huang, A. Verma, D.J. Robles, Q. Wang, P. Mukherjee, J. Sun, Probing the cooling effectiveness of phase change materials on lithium-ion battery thermal response under overcharge condition, *Appl. Therm. Eng.* 132 (2018) 521–530, <https://doi.org/10.1016/j.applthermaleng.2017.12.121>.
- [50] G. Karimi, A.R. Dehghan, Thermal Management Analysis of a Lithium-Ion Battery Pack using Flow Network Approach, vol. 1, 2012. <https://doi.org/10.11159/ijmem.2012.011>.
- [51] R. Ravichandra, S. Rajoo, T.L. Wen, Heat Generation Rate and Computational Simulation for Li-Ion Battery Module, *Int. J. Mech. Mechatron. Eng.* 7 (2013) 989–992.
- [52] N.H.F. Ismail, S.F. Toha, N.A.M. Azubir, N.H. Md Ishak, M. K. Hassan, B.S. Ksm Ibrahim, Simplified heat generation model for lithium-ion battery used in electric vehicle, *IOP Conf. Ser. Mater. Sci. Eng.* 53 (2013) 8–13, <https://doi.org/10.1088/1757-899X/53/1/012014>.

- [53] J. Xu, C. Lan, Y. Qiao, Y. Ma, Prevent thermal runaway of lithium-ion batteries with minichannel cooling, *Appl. Therm. Eng.* 110 (2017) 883–890, <https://doi.org/10.1016/j.applthermaleng.2016.08.151>.
- [54] F. Leng, C.M. Tan, M. Pecht, Effect of Temperature on the Aging rate of Li Ion Battery Operating above Room Temperature, *Sci. Rep.* 5 (2015) 1–12, <https://doi.org/10.1038/srep12967>.
- [55] X. Feng, M. Ouyang, X. Liu, L. Lu, Y. Xia, X. He, Thermal runaway mechanism of lithium-ion battery for electric vehicles: A review, *Energy Storage Mater.* 10 (2018) 246–267, <https://doi.org/10.1016/j.ensm.2017.05.013>.
- [56] Todd M. Bandhauer, Srinivas Garimella, Thomas F. Fuller, A Critical Review of Thermal Issues in Lithium-Ion Batteries, *J. Electrochem. Soc.* 158 (3) (2011) R1, <https://doi.org/10.1149/1.3515880>.
- [57] Rajib Mahamud, Chanwoo Park, Reciprocating air flow for Li-ion battery thermal management to improve temperature uniformity, *J. Power Sources* 196 (13) (2011) 5685–5696, <https://doi.org/10.1016/j.jpowsour.2011.02.076>.
- [58] W. Tong, K. Somasundaram, E. Birgersson, A.S. Mujumdar, C. Yap, Thermo-electrochemical model for forced convection air cooling of a lithium-ion battery module, *Appl. Therm. Eng.* 99 (2016) 672–682, <https://doi.org/10.1016/j.applthermaleng.2016.01.050>.
- [59] Z. Rao, Z. Qian, Y. Kuang, Y. Li, Thermal performance of liquid cooling based thermal management system for cylindrical lithium-ion battery module with variable contact surface, *Appl. Therm. Eng.* 123 (2017) 1514–1522, <https://doi.org/10.1016/j.applthermaleng.2017.06.059>.